

CorrI2P: Deep Image-to-Point Cloud Registration via Dense Correspondence

Siyu Ren, Yiming Zeng, Junhui Hou, *Senior Member, IEEE*, Xiaodong Chen

Abstract—Motivated by the intuition that the critical step of localizing a 2D image in the corresponding 3D point cloud is establishing 2D-3D correspondence between them, we propose the first feature-based dense correspondence framework for addressing the image-to-point cloud registration problem, dubbed CorrI2P, which consists of three modules, i.e., feature embedding, symmetric overlapping region detection, and pose estimation through the established correspondence. Specifically, given a pair of a 2D image and a 3D point cloud, we first transform them into high-dimensional feature space and feed the resulting features into a symmetric overlapping region detector to determine the region where the image and point cloud overlap each other. Then we use the features of the overlapping regions to establish the 2D-3D correspondence before running EPnP within RANSAC to estimate the camera’s pose. Experimental results on KITTI and NuScenes datasets show that our CorrI2P outperforms state-of-the-art image-to-point cloud registration methods significantly. We will make the code publicly available.

Index Terms—Point cloud, registration, cross-modality, correspondence, deep learning.

I. INTRODUCTION

VISUAL pose estimation is a critical task for autopilot [1], robotics [2], and augmented/mixed reality [3] devices since it is the base of SLAM [4], [5] and Structure-from-Motion [6]. Its objective is to determine the image’s 6DOF camera position in a 3D scene. Finding the correspondence between them is the key step in this procedure, followed by utilizing algorithms like EPnP [7] to generate the camera posture based on the relationship.

The registration problem is closely related to visual pose estimation depending on the establishment of correspondence. According to the modality of data, it can be divided into two categories, same-modal, and cross-modal registration. Many solutions for same-modal registration have been presented, such as image-to-image (I2I) [8]–[12] or point cloud-to-point cloud (P2P) registration [13]–[23]. I2I and P2P registration rely on the same-modal correspondence. I2I registration builds 2D-2D correspondence between images, but it only uses color information and could be influenced by the environment. P2P registration builds 3D-3D correspondence between point

clouds, thus it needs large storage space. Both 2D-2D and 3D-3D correspondence are same-modal correspondence. Cross-modal data registration, i.e., image to point cloud (I2P) registration [19], [24], can remedy the disadvantages of these two same-modal techniques. However, it relies on cross-modal correspondence, i.e., 2D-3D correspondence, which is more challenging to estimate. Previous works for I2I and P2P registration focus on establishing same-modal correspondence. However, they cannot be simply extended to establishing 2D-3D correspondence in I2P registration. SfM [6] is a well-known approach for obtaining 2D-3D correspondence, which reconstructs 3D point clouds from a series of images and obtains correspondence based on image features. However, the reconstructed point cloud is not as accurate as the Lidar scanned point cloud. Furthermore, the feature of point cloud is from images, making it susceptible to external influences. 2D3D-MatchNet [24] is the first feature-based registration method, and it finds 2D-3D correspondence directly. However, it focuses on the correspondence of some key points detected by the handcrafted SIFT [25] and ISS [26] features. Then, DeepI2P [19] builds 2D-3D correspondence based on the featureless model. It cast the correspondence problem to frustum classification. However, the points at the frustum boundary are prone to classification errors, limiting registration accuracy.

In this paper, we propose CorrI2P, the first feature-based technique for learning dense 2D-3D correspondence. It is a two-branch neural network with a symmetric cross-attention fusion module identifying overlap and extracting dense features from the image and point cloud. Based on the extracted overlap features, it builds the 2D-3D correspondence and estimates the camera’s posture. We design descriptor loss and detector loss to drive the learning process of CorrI2P. Experimental results show that our CorrI2P achieves state-of-the-art performance on KITTI [27] and NuScenes [28] datasets.

In summary, the main contributions of this paper are three-fold:

- 1) we propose the first feature-based dense correspondence framework for image-to-point cloud registration;
- 2) we design a novel symmetric overlapping region detector for the cross-modal data, i.e., images and point clouds; and
- 3) we propose a joint loss function to drive the learning process of the cross-modal overlap detection and dense correspondence.

The rest of this paper is organized as follows. Sec. II gives a brief review of related work about visual pose estimation

This project was supported in part by the Hong Kong Research Grants Council under Grants 11202320 and 11218121, and in part by the Natural Science Foundation of China under Grant 61871342. *Corresponding author: Junhui Hou*

S. Ren, Y. Zeng, and J. Hou are with the Department of Computer Science, City University of Hong Kong, Hong Kong (email: siyuren2-c@my.cityu.edu.hk; ymzeng4-c@my.cityu.edu.hk; jh.hou@cityu.edu.hk).

X. Chen is with the School of Precision Instrument and Opto-electronics Engineering, Tianjin University, Tianjin, China (email: xdchen@tju.edu.cn).

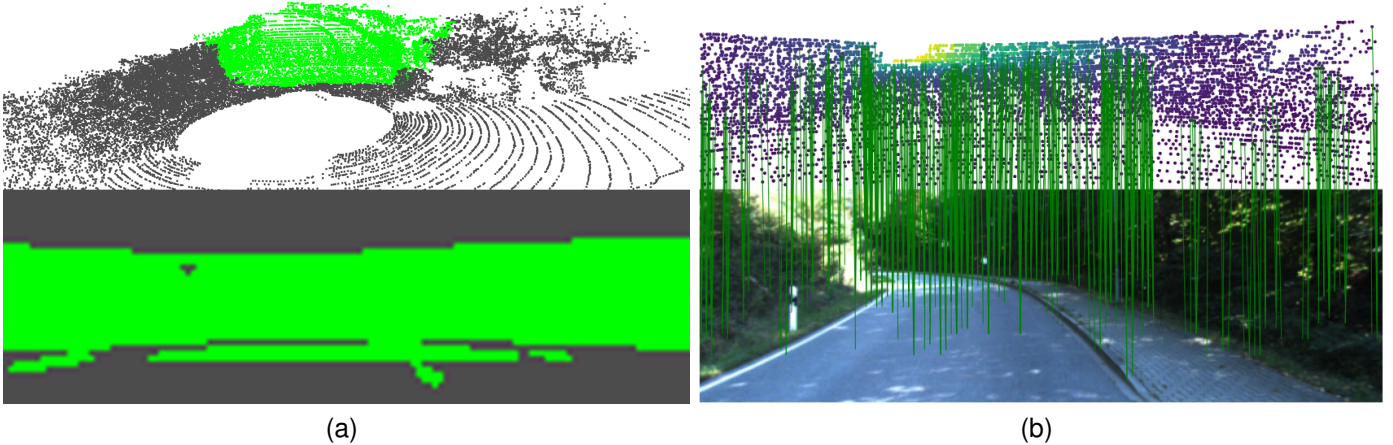


Fig. 1. Illustration of the overlap detection and 2D-3D correspondence between image and point cloud. (a) and (b) are the same pair of data. (a) Overlap Detection: The green pixels and points are detected in the overlapping region of image and point cloud respectively, while those gray ones are not. (b) Dense 2D-3D Correspondence: The point cloud is aligned through ground-truth transformation to visualization, the color of points represent the depth, and the lines represent the 2D-3D correspondence. Here we only show the right correspondence.

and 2D-3D correspondence for registration. Sec. III presents the proposed CorrI2P, followed by extensive experiments and analysis in Sec. IV. Finally, Sec. V concludes this paper.

II. RELATED WORKS

A. Visual Pose Estimation

Given a query image, estimating the 6DOF camera pose in a 3D scene model, usually presented as a point cloud, is crucial for visual navigation. The critical step in this progress is to build 2D-3D correspondence between the image and point cloud. SfM [6] is a traditional method of recovering the point cloud from a sequence of images while using the handcrafted image feature (SIFT [25], ORB [29], or FAST [30]) to generate the 2D-3D correspondence. It utilizes pixel-wise features and the recovered 3D points to establish the 2D-3D correspondence. However, the reconstructed point cloud is sparse, and the imaging environment can affect pixel-wise features.

Some learnable approaches based on same-modal data, i.e., I2I or P2P, have been proposed with the emergence of deep learning. As for the I2I registration methods, [31], [32] collect the images from different environments and train CNNs to extract robust features to establish correspondence. Furthermore, [33]–[35] use CNNs to regress camera pose directly. They benefit from the easy availability of image data but are susceptible to environmental conditions. P2P registration methods, on the other hand, obtain accurate point cloud data from Lidar or RGBD camera.

With the growth of deep learning on the point cloud, [16]–[18], [20], [36]–[40] use neural networks to extract point-wise or global features from the point cloud directly and combine some traditional methods such as RPM [41], RANSAC [42], etc., to estimate the rigid transformation. The above same-modal methods cannot be readily extended to I2P registration, which relies on the learning of 2D-3D correspondence from cross-modal data.

B. 2D-3D Correspondence for Registration

This paper is focused on establishing 2D-3D correspondence on cross-modal data directly to do the registration. The most related works are 2D3D-MatchNet [24] and DeepI2P [19]. Unlike images represented in regular dense grids, 3D point clouds are irregular and unordered, posing substantial challenges to learning correspondence between these two modalities. 2D3D-MatchNet selects key points from the image and point cloud using SIFT [25] and ISS [26], respectively, then feeds the patches around these pixels and points to CNNs [43] and PointNet [44] to extract features for creating 2D-3D correspondence. However, independent key point detection for different modalities will reduce the inlier ratio and registration accuracy. DeepI2P employs a feature-free technique, training a network to do the point-wise frustum classification while optimizing the camera posture using inverse projection until the points identified in the image fall within the frustum. However, at the points near the border of the frustum are easy to get the erroneous classification result. Besides, DeepI2P also divides the image into square regions and uses the network to classify which region the points of the point cloud could be projected onto. The classification result is coarse 2D-3D correspondence, and because of this, the registration accuracy would be low. Another work [45] establishes 2D-3D correspondence, but the pixels and points in the image and point cloud are linear shapes, which is not common 2D-3D correspondence. [46] builds correspondence between 2D and 3D points to estimate the camera pose, but the 2D points are not images taken from the camera, which is different from ours. The methods in [6], [31], [32] establish the 2D-3D correspondence between image and point cloud, but the point cloud is reconstructed from a series of images taken from different locations, and the handcraft or learning-based image feature is used as the point cloud feature rather than from point cloud itself directly, which is different from ours.

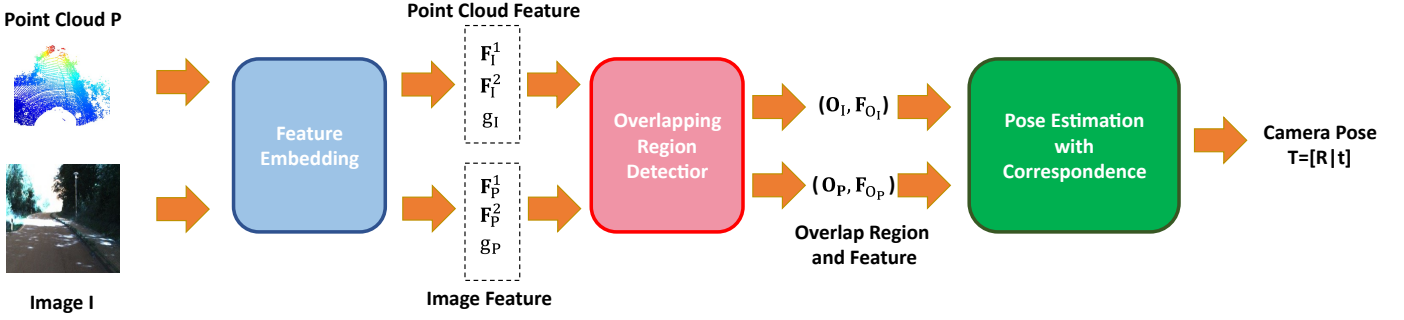


Fig. 2. Illustration of the overall pipeline of the proposed CorrI2P for image-to-point registration.

III. PROPOSED METHOD

Overview. Let $\mathbf{I} \in \mathbb{R}^{W \times H \times 3}$ and $\mathbf{P} \in \mathbb{R}^{N \times 3}$ be a pair of a 2D image and a 3D point cloud, where W and H are the width and height of the image, respectively, and N is the number of points. The objective of I2P registration is to estimate the camera pose in the 3D scene \mathbf{P} , denoted as $\mathbf{T} = [\mathbf{R}|\mathbf{t}]$ with $\mathbf{R} \in \text{SO}(3)$ and $\mathbf{t} \in \mathbb{R}^3$, given a query image \mathbf{I} .

As illustrated in Fig. 2, our method consists of three modules, i.e., feature embedding, symmetric overlapping region detection, and pose estimation with dense correspondence. Specifically, given \mathbf{I} and \mathbf{P} , we first embed them into high-dimensional feature spaces separately, then feed the resulting features into the symmetric overlapping region detector to predict the overlapping region and estimate the dense 2D-3D correspondence, on which we finally run EPnP [7] within RANSAC [42] to estimate the camera pose.

In what follows, we will provide the detail of each module.

A. Feature Embedding

Due to the different structures and characteristics of 2D images and 3D point clouds, it is impossible to deal with them using the same network architecture. Thus, following DeepI2P [19], we utilize ResNet [47] and SO-Net [48] to embed \mathbf{I} and \mathbf{P} to high-dimensional feature spaces in a hierarchical manner, respectively, generating the pixel-wise feature embedding $\mathbf{F}_I^l \in \mathbb{R}^{W_i \times H_i \times d_i}$ and the point-wise feature embedding $\mathbf{F}_P^l \in \mathbb{R}^{N_i \times d_i}$ at the l -th layer ($l = 1, 2$). Then we perform the max-pooling operation on features \mathbf{F}_I^2 and \mathbf{F}_P^2 to obtain the global features of \mathbf{I} and \mathbf{P} , denoted as $\mathbf{g}_I \in \mathbb{R}^d$ and $\mathbf{g}_P \in \mathbb{R}^d$, respectively.

B. Symmetric Overlapping Region Detection

We design a novel symmetric detector to select the overlapping pixels and points to build 2D-3D correspondence. As shown in Fig. 3, we first pass the 2D-3D features into a cross-attention fusion module, composed of two components, namely image-to-point cloud attention fusion (I2PAF) and point cloud-to-image attention fusion (P2IAF), generating weighted features, denoted as $\mathbf{F}_{WI}^l \in \mathbb{R}^{N_i \times d_i}$ and $\mathbf{F}_{WP}^l \in \mathbb{R}^{(H_i \times W_i) \times d_i}$ ($l = 1, 2$), respectively. The underlying intuition is to map the image and point cloud features to each other's space. Then we feed \mathbf{F}_{WI}^l and \mathbf{F}_{WP}^l with the local features (\mathbf{F}_I^l and \mathbf{F}_P^l) into the image and point cloud decoders

and get the overlapping regions, denoted as $\mathbf{O}_I \in \mathbb{R}^{K_I \times 2}$ and $\mathbf{O}_P \in \mathbb{R}^{K_P \times 3}$, and their pixel or point-wise features $\mathbf{F}_{O_I} \in \mathbb{R}^{K_I \times c}$ and $\mathbf{F}_{O_P} \in \mathbb{R}^{K_P \times c}$, where K_I and K_P are the numbers of overlapping pixels and points.

Cross-attention fusion module. As shown in Fig. 4, the cross-attention fusion module consists of the symmetric I2PAF and P2IAF that share a similar structure. This module aims to fuse the information among the image and point cloud such that their overlapping regions can be detected.

For I2PAF, we concatenate the image global feature \mathbf{g}_I and point cloud local feature \mathbf{F}_P^l and feed them into an MLP followed by the Softmax operator to learn the attention weight $\mathbf{W}_{I2P}^l \in \mathbb{R}^{N_i \times (H_i \times W_i)}$. Then we multiply the image local features \mathbf{F}_I^l by attention weights \mathbf{W}_{I2P}^l and finally get the weighted image feature $\mathbf{F}_{WI}^l \in \mathbb{R}^{N_i \times d_i}$. Similar to I2PAF, we can get the weighted point cloud feature $\mathbf{F}_{WP}^l \in \mathbb{R}^{N_i \times d_i}$ using the symmetric module P2IAF.

Image and point cloud decoders. As shown in Fig. 5, the image and point cloud decoders share a similar design. Their intuitions are to recover the spatial dimension using the pixel/point upsampling layers and decrease (or fuse) the feature channels using the ResNet/PointNet layers hierarchically.

After getting weighted features ($\mathbf{F}_{WP}^l, \mathbf{F}_{WI}^l$) and original features ($\mathbf{F}_I^l, \mathbf{F}_P^l$) from previous modules, where the layer $l = 1, 2$, we need to pass them into the decoder to get the overlapping regions of image and point cloud, as well as their features.

For the image decoder shown in Fig. 5a, we first concatenate ($\mathbf{F}_{WP}^2, \mathbf{F}_I^2$) and then feed them into ResNet followed by a pixel upsampling operation (Res&pixelUp) to obtain the feature map $\tilde{\mathbf{F}}_I^1 \in \mathbb{R}^{H_1 \times W_1 \times d_1}$. Then we further concatenate ($\mathbf{F}_{WP}^1, \mathbf{F}_I^1, \tilde{\mathbf{F}}_I^1$) and feed them into another two sets of such operators (Res&pixelUp) to obtain the fused feature map $\tilde{\mathbf{F}}_I \in \mathbb{R}^{H' \times W' \times d'}$. And $\tilde{\mathbf{F}}_I$ will be passed into two CNNs, one CNN for generating the pixel-wise scores $\mathbf{S}_I \in \mathbb{R}^{H' \times W' \times 1}$, another CNN for generating pixel-wise features $\mathbf{H}_I \in \mathbb{R}^{H' \times W' \times c}$. The pixels with higher scores are more likely in the overlapping region, so we set a threshold τ to select these points with higher scores than τ , and their coordinates and features are donated as $\mathbf{O}_I \in \mathbb{R}^{K_I \times 2}$ and $\mathbf{F}_{O_I} \in \mathbb{R}^{K_I \times c}$, respectively, where K_I means the number of overlapping pixels.

The point cloud decoder shown in Fig. 5b shares the same

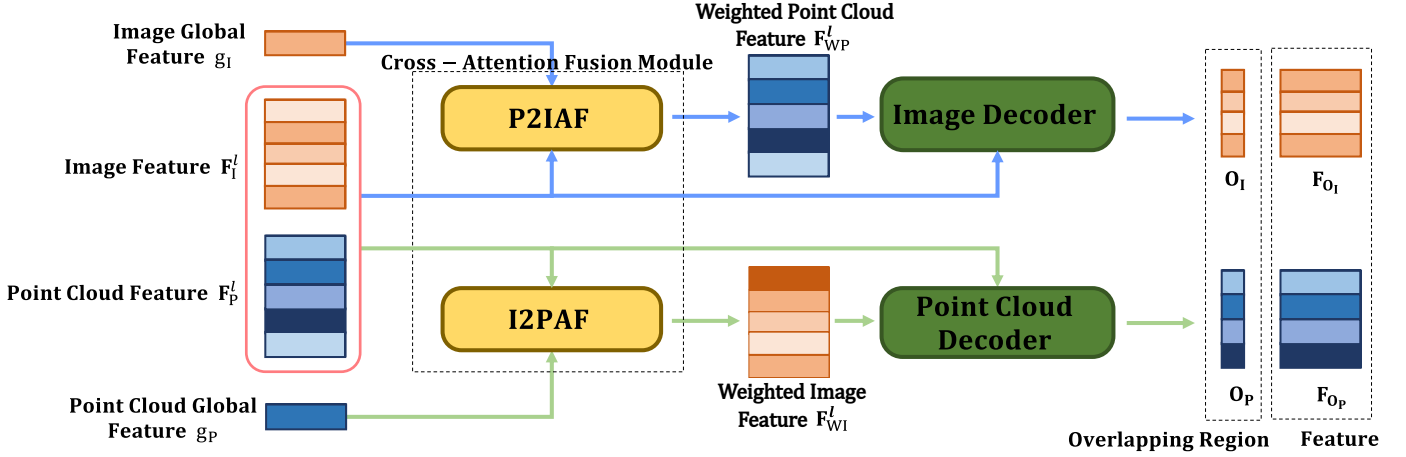


Fig. 3. Illustration of the network architecture of the symmetric overlapping region detector.

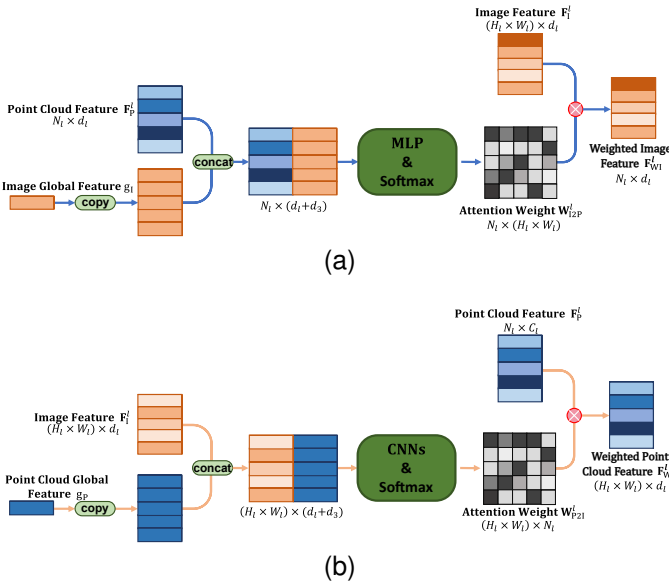


Fig. 4. Illustration of the network architectures of the proposed cross-attention fusion module. (a) Image-to-Point Cloud Attention Fusion Module(I2PAF). (b) Point Cloud-to-Image Attention Fusion Module(P2IAF).

procedure as the image decoder, except that the ResNet is replaced with PointNet, and the pixelUp with pointUp (using PointNet++ [49]), and we pass one set of (PointNet&pointUp) to generate the fused feature map $\tilde{\mathbf{F}}_P \in \mathbb{R}^{N \times d'}$. Also, the CNNs are replaced with PointNet to generate the point-wise scores $\mathbf{S}_P \in \mathbb{R}^{N \times 1}$ and features $\mathbf{H}_P \in \mathbb{R}^{N \times c}$. We use the same threshold τ to filter them and obtain the estimated overlapping region $\mathbf{O}_I \in \mathbb{R}^{K_I \times 3}$ and the corresponding features $\mathbf{F}_{O_P} \in \mathbb{R}^{K_P \times c}$, where K_P means the number of overlapping points.

C. Pose Estimation with Correspondence

Under the assumption that the matched pixel-point pairs have similar features, whereas non-matched pairs have distinct features, we apply the nearest neighbor principle in the feature space of the detected overlapping region to establish 2D-3D correspondence.

Specifically, considering that multiple points of the point cloud may be projected onto an identical pixel of the image, due to occlusion in the scene and the image resolution, we build the 2D-3D correspondence by finding the most similar pixel for each 3D point, i.e., for each point $\mathbf{P}_i \in \mathbf{O}_P$, $i = 1, 2, \dots, K_P$, we select the pixel in the \mathbf{O}_I whose feature is the nearest to that of \mathbf{P}_i as its correspondence. Formally, let $\{\mathbf{I}_{p(i)}, \mathbf{P}_i\}$, $i = 1, 2, \dots, K_P$ be a corresponding pair, where $p(i)$ is the index of the pixel in \mathbf{O}_I , obtained by optimizing

$$p(i) = \arg \min_{j=1,2,\dots,K_I} \|\mathbf{F}_{O_P,i} - \mathbf{F}_{O_I,j}\|. \quad (1)$$

It is inevitable that the above method will generate wrong correspondence, and directly applying the EPnP on them may produce the wrong transformation. Thus, we run EPnP within RANSAC to get the pose of the camera and reject the outliers. Finally, we get the camera pose $\mathbf{T} = [\mathbf{R}|\mathbf{t}]$.

D. Loss Function

To drive the learning process of overlapping region detection and feature matching, we design a joint loss function consisting of a descriptor loss and a detector loss. The descriptor loss is used to constrain the network to learn similar feature pairs and reject the distinct ones. The detection loss guarantees that the network can reliably identify overlap, with higher scores for pixels inside the overlapping zone and lower values for pixels outside the overlapping region.

Descriptor loss. To train the network that outputs descriptors, we adopt the contrastive loss. First, we use the cosine distance to compute the distance in the feature space, i.e.,

$$d(\mathbf{F}_1, \mathbf{F}_2) = 1 - \frac{\langle \mathbf{F}_1, \mathbf{F}_2 \rangle}{\|\mathbf{F}_1\| \|\mathbf{F}_2\|}, \quad (2)$$

where \mathbf{F}_1 and \mathbf{F}_2 represent image or point cloud feature vectors, and $\langle \cdot, \cdot \rangle$ is their inner product.

Given a pair of the image \mathbf{I} and point cloud \mathbf{P} , we use ground truth to sample n pairs of 2D-3D correspondence

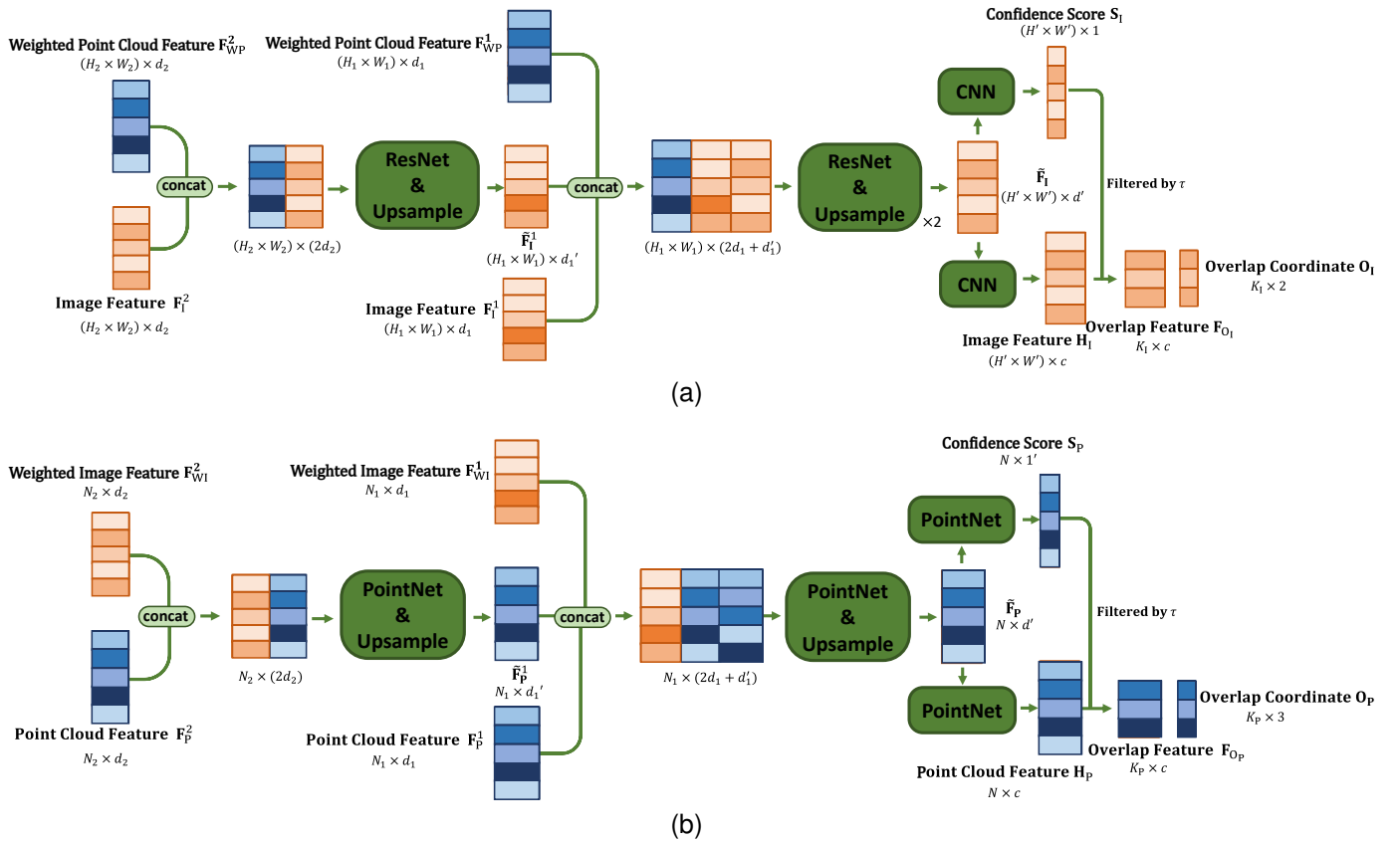


Fig. 5. Illustration of the network architectures of the decoder module. (a) Image Decoder. (b) Point Cloud Decoder.

$\{\mathbf{I}_i, \mathbf{P}_i\}$, $i = 1, 2, \dots, n$ from the overlap, and their corresponding feature pairs are $\{\mathbf{F}_{O_I,i}, \mathbf{F}_{O_P,i}\}$. The feature distance of a positive pair is defined as

$$d_{\text{pos}}(i) = d(\mathbf{F}_{O_I,i}, \mathbf{F}_{O_P,i}). \quad (3)$$

The distance of a negative pair is

$$d_{\text{neg}}(i) = \min_{j=1,2,\dots,n} \{d(\mathbf{F}_{O_I,i}, \mathbf{F}_{O_P,j})\} \text{ s.t. } \|\mathbf{I}_j - \mathbf{I}_i\| > R, \quad (4)$$

where R is the safe radius, and \mathbf{I}_j is the projection of \mathbf{P}_j on the image according to equation. The contrastive margin loss is defined as

$$\mathcal{L}_{\text{desc}} = \frac{1}{n} \sum_{i=1}^n [\max(0, d_{\text{pos}}(i) - M_{\text{pos}}) + \max(0, M_{\text{neg}} - d_{\text{neg}}(i))]. \quad (5)$$

where M_{pos} is the margin for positive pairs and M_{neg} is that for negative pairs.

Detector loss. The detector loss aims at supervising the module for detecting the overlapping regions according to the confidence scores generated from the network. Its objective is to make sure the pixels and points within the overlapping regions have higher scores than those beyond the overlap. We sample n pairs of pixels and points from the overlapping regions with their scores, $\{\mathbf{I}_u, \mathbf{S}_{I,u}\}$, $\mathbf{I}_u \in \mathbf{O}_I$, $u = 1, \dots, n$ and $\{\mathbf{P}_v, \mathbf{S}_{P,v}\}$, $\mathbf{P}_v \in \mathbf{O}_P$, $v = 1, \dots, n$. Besides, we also collect n pixels and points in the non-overlapping region,

$\{\mathbf{I}_k, \mathbf{S}_{I,k}\}$, $\mathbf{I}_k \notin \mathbf{O}_I$, $k = 1, \dots, n$ and $\{\mathbf{P}_m, \mathbf{S}_{P,m}\}$, $\mathbf{P}_m \notin \mathbf{O}_P$, $m = 1, \dots, n$. The detector loss is defined as

$$\mathcal{L}_{\text{det}} = \frac{1}{n} \left(- \sum_{u=1}^n \mathbf{S}_{I,u} - \sum_{v=1}^n \mathbf{S}_{P,v} + \sum_{k=1}^n \mathbf{S}_{I,k} + \sum_{m=1}^n \mathbf{S}_{P,m} \right). \quad (6)$$

In total, our loss function is

$$\mathcal{L} = \mathcal{L}_{\text{desc}} + \lambda \mathcal{L}_{\text{det}}, \quad (7)$$

where λ is a hyperparameter and used to balance the two terms.

IV. EXPERIMENTS

We adopt two commonly used datasets, i.e., KITTI [27] and NuScenes [28], to evaluate the proposed method.

- **KITTI Odometry** [27]. Point clouds are directly acquired from a 3D Lidar. The image-point cloud pairs are selected from the same data frame, i.e., a pair of image and point cloud is from the same data frame. The images are facing the front. We follow the common practice of utilizing the 0-8 sequences for training and 9-10 for testing. The transformation of the point cloud consists a rotation around the up-axis and 2D translation on the ground within the range of 10m. During training, the size of the image is 160×512 , while the number of points is 40960.

- **NuScenes** [28]. Point clouds are acquired from a Lidar with a full 360-degree field of view. We use the official SDK to get the image-point cloud pairs, where the point cloud is accumulated from the nearby frames, and the image is from the current data frame. We follow the official data split of NuScenes, which is that 850 scenes are used for training, and 150 are used for testing, and the range of transformation is similar to the KITTI dataset. The image size is 160×320 , and the number of points is the same as the KITTI dataset.

B. Implementation Details

Training. During training, we establish the ground truth 2D-3D correspondence to supervise the network, and the transformation of a point $\mathbf{P}_i \in \mathbb{R}^3$ in the point cloud to image coordinate of the camera $\mathbf{p}_i \in \mathbb{R}^2$ is given by

$$\tilde{\mathbf{p}}_i = \begin{bmatrix} x'_i \\ y'_i \\ z'_i \end{bmatrix} = \mathbf{K}(\mathbf{R}_{\text{gt}}\mathbf{P}_i + \mathbf{t}_{\text{gt}}), \quad (8)$$

$$\mathbf{p}_i = \begin{bmatrix} p_{xi} \\ p_{yi} \end{bmatrix} = \begin{bmatrix} x'_i/z'_i \\ y'_i/z'_i \end{bmatrix}, \quad (9)$$

where $\mathbf{K} \in \mathbb{R}^{3 \times 3}$ is the camera intrinsic matrix and $\mathbf{T}_{\text{gt}} = [\mathbf{R}_{\text{gt}}|\mathbf{t}_{\text{gt}}]$ is the ground truth camera pose.

For image features, \mathbf{I}_1 is 1/16 scale of the original image while \mathbf{I}_2 is 1/32, and the final feature map \mathbf{H}_1 is 1/4, e.i., $W = 16W_1 = 32W_2 = 4W'$. As for point cloud features, $N_1 = N_2 = 256$, and the number of k-NN nearest neighborhood in SO-Net is $k = 32$. The feature channels are $d_1 = d'_1 = 256$, $d_2 = d_3 = 512$ and $c = 128$. For each dataset, we train our network for 25 epochs, with batch size of 24. We use the Adam [50] to optimize the network, and the initial learning rate is 0.001 and multiplied by 0.25 every 5 epochs until it is 0.00001. During the training, the safe radius R is 1 pixel. The λ in loss function is set to 0.5, the positive margin is $M_{\text{pos}} = 0.2$, negative margin is $M_{\text{neg}} = 1.8$, and the safe radius $R = 1$ pixel.

Testing. During testing, we use a pair of image and point cloud as input to our network and set $\tau = 0.9$ to obtain the overlapping regions and their corresponding features. Then we establish 2D-3D correspondence and use EPnP within RANSAC to get the camera pose and reject the outliers. The number of iterations is set as 500, and the threshold for inlier reprojection error is 1 pixel.

C. Compared Methods

We choose Grid Cls. + PnP. and Frus. Cls. + Inv.Proj. as our compared methods.

- **Grid Cls. + PnP.** proposed in DeepI2P [19], the most recent work on this topic, divides the image into 32×32 grids and uses the network to classify each point in the point cloud belonging to which grid of the image. It establishes 2D-3D correspondence based on the classification result then uses EPnP with RANSAC to estimate the camera pose.

- **Frus. Cls. + Inv.Proj.** uses the frustum classification and inverse camera projection in DeepI2P [19] to obtain the camera pose. We use the same network setting as their paper and try the 2D and 3D inverse camera projection to optimize the pose, and they are represented by DeepI2P(2D) and DeepI2P(3D), respectively. We use a 60-fold random initialization to search for the initial pose of the camera.

Evaluation metric. Similar to P2P registration [51], we use Relative Translational Error (RTE) E_t and Relative Rotational Error (RRE) E_R to evaluate our registration result, which are computed as

$$E_R = \sum_{i=1}^3 |\gamma(i)|, \quad (10)$$

$$E_t = \|\mathbf{t}_{\text{gt}} - \mathbf{t}_{\text{E}}\|, \quad (11)$$

where γ is the Euler angle of the matrix $\mathbf{R}_{\text{gt}}^{-1}\mathbf{R}_{\text{E}}$, \mathbf{R}_{gt} and \mathbf{t}_{gt} are the ground-truth transformation, and \mathbf{R}_{E} and \mathbf{t}_{E} are the estimated transformation.

In the ablation study, we also conduct a feature matching experiment to show the quality of the correspondence estimator. Inspired by the P2P registration [52], we design two kinds of recall to evaluate the feature matching. Pair recall R_{pair} recall is the ratio of the correct correspondences, while fragment recall R_{frag} is the ratio of the fragments whose correct 2D-3D correspondences is a higher proportion than a pre-set threshold. They are calculated as

$$R_{\text{pair}} = \frac{1}{M} \sum_{s=1}^M \left(\frac{1}{|\mathbf{O}_{\text{p}}^s|} \sum_{i \in \mathbf{O}_{\text{p}}^s} \mathbb{1}(\|\mathbf{p}_{p(i)}^s - \pi(\mathbf{T}_{\text{gt}}^s \mathbf{P}_i^s)\| < \tau_1) \right), \quad (12)$$

$$R_{\text{frag}} = \frac{1}{M} \sum_{s=1}^M \mathbb{1} \left(\left(\frac{1}{|\mathbf{O}_{\text{p}}^s|} \sum_{i \in \mathbf{O}_{\text{p}}^s} \mathbb{1}(\|\mathbf{p}_{p(i)}^s - \pi(\mathbf{T}_{\text{gt}}^s \mathbf{P}_i^s)\| < \tau_1) \right) > \tau_2 \right), \quad (13)$$

where τ_1 and τ_2 are the inlier distance and inlier ration threshold, M is the number of ground truth matching image-point cloud pairs, $\pi(\cdot)$ is the projection from point cloud to image coordinate according to eq(8)(9), $\mathbb{1}(\cdot)$ is the indicator function, and \mathbf{T}_{gt}^s is the ground truth transformation of the s -th image-point cloud pair. \mathbf{p} is the pixel coordinate, and \mathbf{P} is the point cloud coordinate. $p(i)$ is the index of i -th point in the point cloud's corresponding pixel using Eq. (1).

D. Results

Registration accuracy. The registration accuracy is illustrated in Tab. I. Note that some failed registration results may cause dramatically large RRE and RTE, which would show unreliable error metrics. Similar to P2P registration [53], [54], the average RTE and RRE are only calculated for those with RTE lower than 5m and RRE lower than 10° . From Tab. I, it can be seen that our method outperforms all compared methods by a noticeable margin on both two datasets. Besides, for a more detailed comparison of the registration performance, we show

TABLE I

COMPARISON OF THE REGISTRATION ACCURACY (MEAN \pm STD) OF DIFFERENT METHODS ON THE KITTI AND NuScenes DATASETS. “ \downarrow ” MEANS THAT THE SMALLER, THE BETTER.

	KITTI		NuScenes	
	RTE \downarrow (m)	RRE \downarrow ($^\circ$)	RTE \downarrow (m)	RRE \downarrow ($^\circ$)
Grid Cls. + EPnP [19]	1.07 \pm 0.61	6.48 \pm 1.66	2.35 \pm 1.12	7.20 \pm 1.65
DeepI2P (3D) [19]	1.27 \pm 0.80	6.26 \pm 2.29	2.00 \pm 1.08	7.18 \pm 1.92
DeepI2P (2D) [19]	1.46 \pm 0.96	4.27 \pm 2.74	2.19 \pm 1.16	3.54 \pm 2.51
Ours	0.74 \pm 0.65	2.07 \pm 1.64	1.83 \pm 1.06	2.65 \pm 1.93

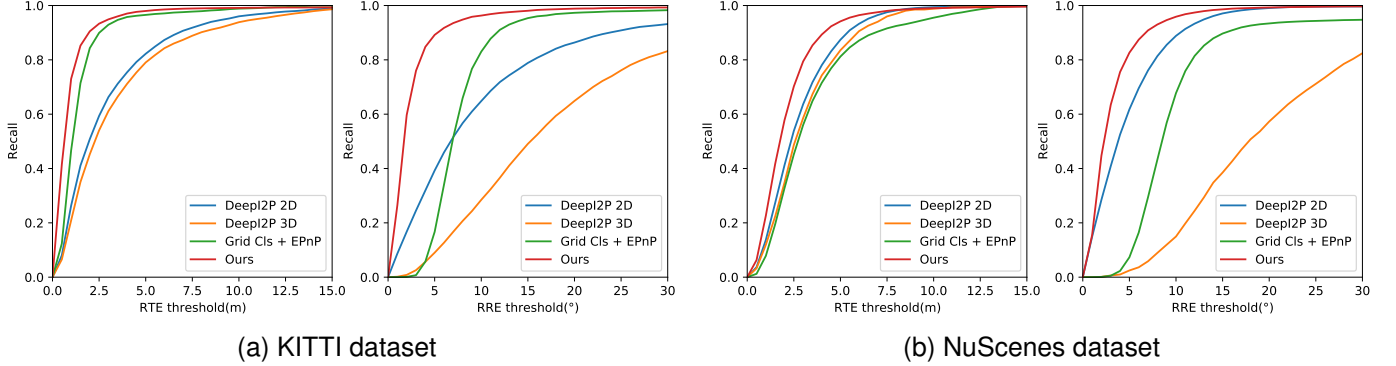


Fig. 6. Registration recall with different RTE and RRE thresholds on KITTI dataset and NuScenes dataset.

the registration recall with different RTE and RRE thresholds on two datasets in Fig. 6.

Although the frustum classification accuracy achieves 0.97 on both datasets, DeepI2P still achieves worse performance than our CorrI2P, because the points located in the frustum are very easy to be wrongly classified, which has an adverse influence on the inverse camera projection and eventually gets the wrong camera pose. Grid Cls. + EPnP has worse registration accuracy because the 32×32 grid size is too coarse to get an accurate pose, although the grid classification accuracy achieves 0.50.

Error distribution. The distributions of the registration error, i.e., RTE and RRE, are shown in Fig. 7, where it can be seen that the performance is better on KITTI than NuScenes. The mode of RTE/RRE is $0.5\text{m}/2^\circ$ on KITTI and $1.5\text{m}/2^\circ$ on NuScenes. The RTE and RRE variances are also smaller on KITTI.

Overlapping region detection accuracy. In the image and point cloud decoders, we use threshold τ to filter the pixels and points in image and point cloud, regarding them located in the overlapping regions. This can be seen as a classification process. Thus, we use recall, precision, and F2-score on KITTI dataset to evaluate the performance of our overlapping region detection. Similar to 2D3DMatchNet [24], we use Random, SIFT and ISS to extract the keypoints in image and point cloud as overlapping region detection. For random sample, we sample 2048 pixels and 8192 points from image and point cloud, respectively. Besides, we also use the frustum classifier

of point cloud in DeepI2P as a comparison. The results are listed in Tab. II, the detection accuracy of Random, SIFT, and ISS is much worse than ours. The reason is that these method select pixels or points in the whole image and point cloud, but their ground truth overlapping regions only take up small proportion, resulting in less correct correspondence and lower registration. The accuracy of registration based on these overlapping region detection method would be shown in the ablation study. It can also be seen that our method for point cloud is better than DeepI2P. The precision of our overlapping region detection is higher than 0.9 on both image and point cloud, which ensures the accuracy of registration.

TABLE II
THE PERFORMANCE OF OVERLAP DETECTION ON KITTI DATASET.

	Method	Recall	Precision	F2-Score
PC	ISS [26]	0.044	0.268	0.076
	Random	0.199	0.196	0.197
	DeepI2P [19]	0.935	0.946	0.938
	Ours	0.975	0.911	0.941
IMG	SIFT [25]	0.091	0.585	0.156
	Random	0.329	0.599	0.424
	Ours	0.783	0.903	0.838

KITTI vs. NuScenes. Our registration accuracy is higher on KITTI than NuScenes dataset. The main reason is that the point clouds of the scene in the two datasets are acquired through different methods. The point cloud in the KITTI dataset is dense enough, and it doesn’t need to be spliced

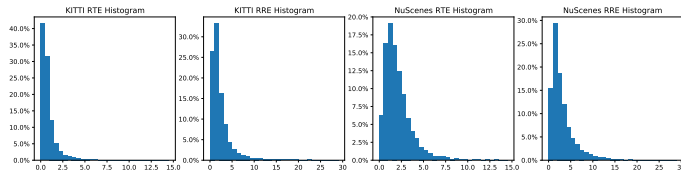


Fig. 7. Histograms of RTE and RRE on the KITTI and NuScenes datasets. x-axis is RTE(m) and RRE($^{\circ}$), and y-axis is the percentage.

with another frame. As for NuScenes dataset, every point cloud frame is too sparse to use directly, so we need to splice it with the adjacent frames. However, the point cloud is collected on the street, and some components in the scenes are dynamic, such as cars or pedestrians, making the point cloud not aligned completely, and it would cause trouble when extracting point cloud features.

E. Ablation Study

In this section, we conducted ablation studies for our Corri2P. We carried out the experiments on the KITTI dataset. **Cross-attention Fusion Module.** The cross-attention module can fuse the information from different modality data, i.e., image and point cloud in each other. It helps not only overlap detection but also feature extraction as well as correspondence estimation, so it is an essential part of our network. To identify this, we conduct the ablation study about it. Similar to P2P registration [55], we train a network without cross attention fusion module and detection loss and use pair recall R_{pair} and fragment recall R_{frag} defined in eq(12)(13) to evaluate the 2D-3D feature matching. The result is shown in Fig. 8a, we plot the recall about inlier distance and inlier ratio threshold. i.e., τ_1 and τ_2 . The pair recall changes with different τ_1 , and for fragment recall, we set $\tau_1 = 1$ pixel and show how it would change along with τ_2 . The result illustrates that the image and point cloud feature would worsen 2D-3D correspondence accuracy without cross-attention fusion module.

TABLE III
COMPARISON OF THE REGISTRATION ACCURACY OF DIFFERENT SAMPLING STRATEGIES ON KITTI DATASET.

IMG	PC	RTE (m)	RRE ($^{\circ}$)
Random	Random	1.57 ± 1.01	3.53 ± 2.22
Random	Score	0.94 ± 0.71	3.06 ± 1.85
Score	Random	1.79 ± 1.14	3.67 ± 2.19
Score	ISS	1.67 ± 1.08	3.40 ± 2.12
SIFT	Score	0.94 ± 0.71	2.89 ± 1.88
SIFT	ISS	1.91 ± 1.15	4.13 ± 2.25
Score	Score	0.74 ± 0.65	2.07 ± 1.64

Overlapping region detection. Our Corri2P can detect the overlapping region of the image and point cloud and use the pixels and points from the overlapping region to estimate the camera pose. This can increase the inlier ratio of 2D-3D correspondence, thus achieving higher registration accuracy. To verify this, we employ different sampling strategies during the

registration, such as random and keypoint selection. We only use descriptor loss to train the network for these experiments because the confidence score is not used. For random strategy, we keep the same number of sampled pixels and points, i.e., we randomly select 2048 pixels and 8192 points from the image and point cloud, respectively, as well as their features to do the registration. For keypoint selection, we imitate 2D3D-MatchNet, use SIFT and ISS to detect the key points from the image and point cloud to do registration. We use 'Score' to represent our overlapping region detector because we use a confidence score to select the pixels and points. Besides, we also mix these sampling strategies with ours, such as 'IMG Random' and 'PC Score'. The result is shown in Fig. 8b and Tab. III. It can be seen that without our overlapping region detection, the registration accuracy would significantly decrease. However, only by removing the overlap detection for image, i.e., 'IMG Random + PC Score' or 'IMG SIFT + PC Score', the accuracy would decrease only a little while removing that for point cloud, i.e. 'PC Random' or 'PC ISS' the registration performance would decrease significantly. It is that the points that can be projected onto the image only take up a small part of the whole point cloud, while overlap region on image accounts for a large proportion. This can be seen from the Fig. 1a.

TABLE IV
COMPARISON OF THE REGISTRATION ACCURACY OF DIFFERENT 3D POINT DENSITY.

# points	RTE (m)	RRE ($^{\circ}$)
5120	1.19 ± 0.87	2.72 ± 1.91
10240	1.08 ± 0.83	2.59 ± 1.91
20480	0.93 ± 0.77	2.26 ± 1.77
40960	0.74 ± 0.65	2.07 ± 1.64

3D point cloud density. Considering that the density of 3D point clouds is a key factor in feature extraction, we carry out the ablation experiment on it. For a scene of the same size, we change the density of the point cloud by downsampling different numbers of points. In order to keep the same receptive fields for point cloud with different point densities, we scale the numbers of knn searching for different densities, i.e., $k = 32$ for 40960 points, $k = 16$ for 20480 points, and $k = 8$ for 10240 and 5120 points. The result is shown in Tab. IV, the registration accuracy decreases with reducing 3D point density because point cloud in low density would omit some structure information, and the feature extracted would be less descriptive, resulting in wrong 2D-3D correspondence and thus low registration accuracy.

F. Running Time

We use the KITTI dataset to evaluate the efficiency of our Corri2P. We use an NVIDIA GeForce RTX 3090 GPU for neural network inference and Intel(R) Xeon(R) Gold 6346 CPU for pose estimation. We feed data with a batch size of 8 to the neural network and get the average inference time. The result is shown in Tab. V. It can be seen that classification

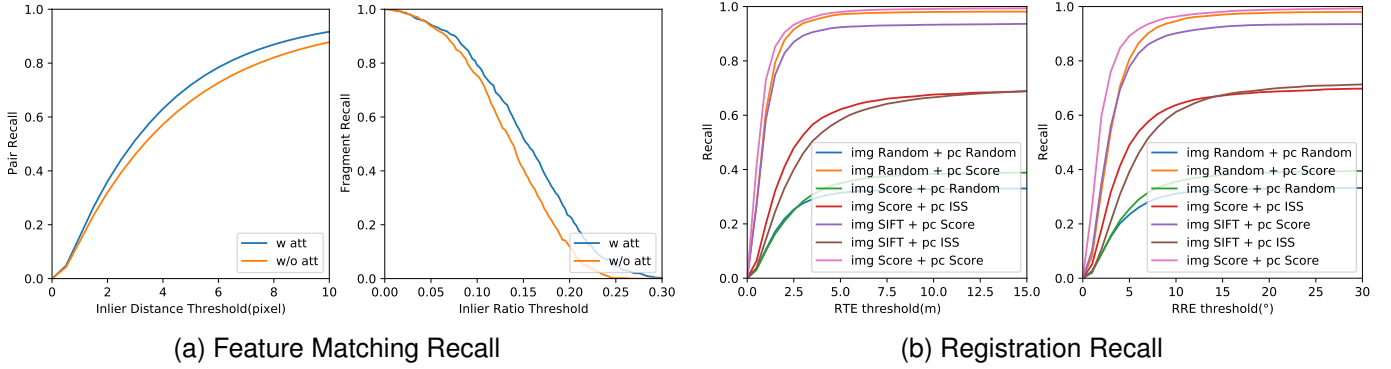


Fig. 8. Ablation study result on KITTI dataset. (a) Feature matching recall in relation to inlier ratio threshold τ_1 (left) and inlier ratio threshold τ_2 (right). (b) Registration recall with different RTE and RRE thresholds.

methods, i.e., Grid Cls. and DeepI2P, are faster than ours in the inference because our network needs to do feature extraction of image and point cloud, rather than only classify the points of the point cloud. As for pose estimation, Grid Cls. + EPnP is the fastest because the image grid is 32×32 resulting in a higher inlier ratio than ours and the RANSAC only needs fewer iterations. DeepI2P is much slower than other methods because it needs 60-fold pose initialization before the optimization to enhance the robustness.

TABLE V
COMPARISON OF THE AVERAGE RUNNING TIME OF DIFFERENT METHODS ON THE KITTI DATASET.

Method	Inference (ms)	Pose Estimation (s)
Grid Cls. + EPnP	11.20	0.04
DeepI2P (3D)	7.55	16.58
DeepI2P (2D)	7.58	9.38
Ours	13.75	2.97

V. CONCLUSION

We have presented the first feature-based dense correspondence framework named CorrI2P for image-to-point cloud registration. Unlike existing works, we designed a symmetric overlapping region detector for images and point clouds. We demonstrated the significant advantages of our method over state-of-the-art ones by conducting extensive experiments on the KITTI and NuScenes datasets, as well as comprehensive ablation studies. We believe our methods will benefit to other tasks, such as distillation on image or point cloud and semantic segmentation for cross-modality data, which usually transform the different kinds of data to the same feature space.

REFERENCES

- [1] M. Rizk, A. Mroue, M. Farran, and J. Charara, "Real-time slam based on image stitching for autonomous navigation of uavs in gnss-denied regions," in *2020 2nd IEEE International Conference on Artificial Intelligence Circuits and Systems (AICAS)*. IEEE, 2020, pp. 301–304.
- [2] P. Mühlfellner, M. Bürki, M. Bosse, W. Derendarz, R. Philippsen, and P. Furgale, "Summary maps for lifelong visual localization," *Journal of Field Robotics*, vol. 33, no. 5, pp. 561–590, 2016.
- [3] J. T. Verhey, J. M. Haglin, E. M. Verhey, and D. E. Hartigan, "Virtual, augmented, and mixed reality applications in orthopedic surgery," *The International Journal of Medical Robotics and Computer Assisted Surgery*, vol. 16, no. 2, p. e2067, 2020.
- [4] H. Durrant-Whyte and T. Bailey, "Simultaneous localization and mapping: part i," *IEEE robotics & automation magazine*, vol. 13, no. 2, pp. 99–110, 2006.
- [5] H. Zhang and J. Peng, "Visual slam location methods based on complex scenes: A review," in *International Conference on Artificial Intelligence and Security*. Springer, 2020, pp. 487–498.
- [6] S. Agarwal, Y. Furukawa, N. Snavely, I. Simon, B. Curless, S. M. Seitz, and R. Szeliski, "Building rome in a day," *Communications of the ACM*, vol. 54, no. 10, pp. 105–112, 2011.
- [7] V. Lepetit, F. Moreno-Noguer, and P. Fua, "Epnp: An accurate o (n) solution to the pnp problem," *International journal of computer vision*, vol. 81, no. 2, pp. 155–166, 2009.
- [8] A. Sotiras, C. Davatzikos, and N. Paragios, "Deformable medical image registration: A survey," *IEEE transactions on medical imaging*, vol. 32, no. 7, pp. 1153–1190, 2013.
- [9] B. S. Reddy and B. N. Chatterji, "An fft-based technique for translation, rotation, and scale-invariant image registration," *IEEE transactions on image processing*, vol. 5, no. 8, pp. 1266–1271, 1996.
- [10] C. Domokos, Z. Kato, and J. M. Francos, "Parametric estimation of affine deformations of binary images," in *2008 IEEE International Conference on Acoustics, Speech and Signal Processing*. IEEE, 2008, pp. 889–892.
- [11] I.-H. Lee and T.-S. Choi, "Accurate registration using adaptive block processing for multispectral images," *IEEE transactions on circuits and systems for video technology*, vol. 23, no. 9, pp. 1491–1501, 2013.
- [12] M. N. Haque, M. Biswas, M. R. Pickering, and M. R. Frater, "A low-complexity image registration algorithm for global motion estimation," *IEEE transactions on circuits and systems for video technology*, vol. 22, no. 3, pp. 426–433, 2011.
- [13] P. J. Besl and N. D. McKay, "Method for registration of 3-d shapes," in *Sensor fusion IV: control paradigms and data structures*, vol. 1611. Spie, 1992, pp. 586–606.
- [14] Q.-Y. Zhou, J. Park, and V. Koltun, "Fast global registration," in *European conference on computer vision*. Springer, 2016, pp. 766–782.
- [15] J. Yang, H. Li, and Y. Jia, "Go-icp: Solving 3d registration efficiently and globally optimally," in *Proceedings of the IEEE International Conference on Computer Vision*, 2013, pp. 1457–1464.
- [16] A. Zeng, S. Song, M. Nießner, M. Fisher, J. Xiao, and T. Funkhouser, "3dmatch: Learning local geometric descriptors from rgb-d reconstructions," in *Proceedings of the IEEE conference on computer vision and pattern recognition*, 2017, pp. 1802–1811.
- [17] Z. Gojcic, C. Zhou, J. D. Wegner, and A. Wieser, "The perfect match: 3d point cloud matching with smoothed densities," in *Proceedings of the IEEE/CVF conference on computer vision and pattern recognition*, 2019, pp. 5545–5554.
- [18] S. Huang, Z. Gojcic, M. Usvatsov, A. Wieser, and K. Schindler, "Predator: Registration of 3d point clouds with low overlap," in *Proceedings of the IEEE/CVF Conference on computer vision and pattern recognition*, 2021, pp. 4267–4276.

- [19] J. Li and G. H. Lee, "Deepi2p: Image-to-point cloud registration via deep classification," in *Proceedings of the IEEE/CVF Conference on Computer Vision and Pattern Recognition*, 2021, pp. 15 960–15 969.
- [20] W. Lu, G. Wan, Y. Zhou, X. Fu, P. Yuan, and S. Song, "Deepicp: An end-to-end deep neural network for 3d point cloud registration [j]," in *IEEE ICCV*, 2019.
- [21] X. Huang, J. Zhang, Q. Wu, L. Fan, and C. Yuan, "A coarse-to-fine algorithm for matching and registration in 3d cross-source point clouds," *IEEE Transactions on Circuits and Systems for Video Technology*, vol. 28, no. 10, pp. 2965–2977, 2017.
- [22] J. Yang, Z. Huang, S. Quan, Q. Zhang, Y. Zhang, and Z. Cao, "Toward efficient and robust metrics for ransac hypotheses and 3d rigid registration," *IEEE Transactions on Circuits and Systems for Video Technology*, vol. 32, no. 2, pp. 893–906, 2021.
- [23] J. Yang, Y. Xiao, and Z. Cao, "Aligning 2.5 d scene fragments with distinctive local geometric features and voting-based correspondences," *IEEE Transactions on Circuits and Systems for Video Technology*, vol. 29, no. 3, pp. 714–729, 2018.
- [24] M. Feng, S. Hu, M. H. Ang, and G. H. Lee, "2d3d-matchnet: Learning to match keypoints across 2d image and 3d point cloud," in *2019 International Conference on Robotics and Automation (ICRA)*. IEEE, 2019, pp. 4790–4796.
- [25] D. G. Lowe, "Object recognition from local scale-invariant features," in *Proceedings of the seventh IEEE international conference on computer vision*, vol. 2. Ieee, 1999, pp. 1150–1157.
- [26] Y. Zhong, "Intrinsic shape signatures: A shape descriptor for 3d object recognition," in *2009 IEEE 12th international conference on computer vision workshops, ICCV Workshops*. IEEE, 2009, pp. 689–696.
- [27] A. Geiger, P. Lenz, C. Stiller, and R. Urtasun, "Vision meets robotics: The kitti dataset," *The International Journal of Robotics Research*, vol. 32, no. 11, pp. 1231–1237, 2013. [Online]. Available: <https://doi.org/10.1177/0278364913491297>
- [28] H. Caesar, V. Bankiti, A. H. Lang, S. Vora, V. E. Liong, Q. Xu, A. Krishnan, Y. Pan, G. Baldan, and O. Beijbom, "nusenes: A multimodal dataset for autonomous driving," in *Proceedings of the IEEE/CVF conference on computer vision and pattern recognition*, 2020, pp. 11 621–11 631.
- [29] E. Rublee, V. Rabaud, K. Konolige, and G. Bradski, "Orb: An efficient alternative to sift or surf," in *2011 International conference on computer vision*. Ieee, 2011, pp. 2564–2571.
- [30] E. Rosten and T. Drummond, "Machine learning for high-speed corner detection," in *European conference on computer vision*. Springer, 2006, pp. 430–443.
- [31] Z. Chen, A. Jacobson, N. Sünderhauf, B. Upcroft, L. Liu, C. Shen, I. Reid, and M. Milford, "Deep learning features at scale for visual place recognition," in *2017 IEEE International Conference on Robotics and Automation (ICRA)*. IEEE, 2017, pp. 3223–3230.
- [32] P. Mühlfellner, M. Bürki, M. Bosse, W. Derendarz, R. Philippsen, and P. Furgale, "Summary maps for lifelong visual localization," *Journal of Field Robotics*, vol. 33, no. 5, pp. 561–590, 2016.
- [33] R. Clark, S. Wang, A. Markham, N. Trigoni, and H. Wen, "Vidloc: A deep spatio-temporal model for 6-dof video-clip relocalization," in *Proceedings of the IEEE Conference on Computer Vision and Pattern Recognition*, 2017, pp. 6856–6864.
- [34] A. Kendall, M. Grimes, and R. Cipolla, "Posenet: A convolutional network for real-time 6-dof camera relocalization," in *Proceedings of the IEEE international conference on computer vision*, 2015, pp. 2938–2946.
- [35] F. Walch, C. Hazirbas, L. Leal-Taixe, T. Sattler, S. Hilsenbeck, and D. Cremers, "Image-based localization using lstms for structured feature correlation," in *Proceedings of the IEEE International Conference on Computer Vision*, 2017, pp. 627–637.
- [36] Y. Wang and J. M. Solomon, "Deep closest point: Learning representations for point cloud registration," in *Proceedings of the IEEE/CVF international conference on computer vision*, 2019, pp. 3523–3532.
- [37] Z. J. Yew and G. H. Lee, "Rpm-net: Robust point matching using learned features," in *Proceedings of the IEEE/CVF conference on computer vision and pattern recognition*, 2020, pp. 11 824–11 833.
- [38] X. Bai, Z. Luo, L. Zhou, H. Fu, L. Quan, and C.-L. Tai, "D3feat: Joint learning of dense detection and description of 3d local features," in *Proceedings of the IEEE/CVF conference on computer vision and pattern recognition*, 2020, pp. 6359–6367.
- [39] Y. Aoki, H. Goforth, R. A. Srivatsan, and S. Lucey, "Pointnetlk: Robust & efficient point cloud registration using pointnet," in *Proceedings of the IEEE/CVF conference on computer vision and pattern recognition*, 2019, pp. 7163–7172.
- [40] V. Sarode, X. Li, H. Goforth, Y. Aoki, R. A. Srivatsan, S. Lucey, and H. Choset, "Pcnet: Point cloud registration network using pointnet encoding," *arXiv preprint arXiv:1908.07906*, 2019.
- [41] A. W. Fitzgibbon, "Robust registration of 2d and 3d point sets," *Image and Vision Computing*, vol. 21, no. 13, pp. 1145–1153, 2003, british Machine Vision Computing 2001. [Online]. Available: <https://www.sciencedirect.com/science/article/pii/S0262885603001835>
- [42] M. A. Fischler and R. C. Bolles, "Random sample consensus: a paradigm for model fitting with applications to image analysis and automated cartography," *Communications of the ACM*, vol. 24, no. 6, pp. 381–395, 1981.
- [43] K. Simonyan and A. Zisserman, "Very deep convolutional networks for large-scale image recognition," *arXiv preprint arXiv:1409.1556*, 2014.
- [44] C. R. Qi, H. Su, K. Mo, and L. J. Guibas, "Pointnet: Deep learning on point sets for 3d classification and segmentation," in *Proceedings of the IEEE conference on computer vision and pattern recognition*, 2017, pp. 652–660.
- [45] H. Yu, W. Zhen, W. Yang, J. Zhang, and S. Scherer, "Monocular camera localization in prior lidar maps with 2d-3d line correspondences," in *2020 IEEE/RSJ International Conference on Intelligent Robots and Systems (IROS)*. IEEE, 2020, pp. 4588–4594.
- [46] L. Liu, D. Campbell, H. Li, D. Zhou, X. Song, and R. Yang, "Learning 2d-3d correspondences to solve the blind perspective-n-point problem," *arXiv preprint arXiv:2003.06752*, 2020.
- [47] K. He, X. Zhang, S. Ren, and J. Sun, "Deep residual learning for image recognition," in *Proceedings of the IEEE conference on computer vision and pattern recognition*, 2016, pp. 770–778.
- [48] J. Li, B. M. Chen, and G. H. Lee, "So-net: Self-organizing network for point cloud analysis," in *Proceedings of the IEEE conference on computer vision and pattern recognition*, 2018, pp. 9397–9406.
- [49] C. R. Qi, L. Yi, H. Su, and L. J. Guibas, "Pointnet++: Deep hierarchical feature learning on point sets in a metric space," *Advances in neural information processing systems*, vol. 30, 2017.
- [50] D. P. Kingma and J. Ba, "Adam: A method for stochastic optimization," 2015.
- [51] Y. Ma, Y. Guo, J. Zhao, M. Lu, J. Zhang, and J. Wan, "Fast and accurate registration of structured point clouds with small overlaps," in *Proceedings of the IEEE Conference on Computer Vision and Pattern Recognition Workshops*, 2016, pp. 1–9.
- [52] M. Khoury, Q.-Y. Zhou, and V. Koltun, "Learning compact geometric features," in *Proceedings of the IEEE international conference on computer vision*, 2017, pp. 153–161.
- [53] X. Bai, Z. Luo, L. Zhou, H. Chen, L. Li, Z. Hu, H. Fu, and C.-L. Tai, "Pointdsc: Robust point cloud registration using deep spatial consistency," in *Proceedings of the IEEE/CVF Conference on Computer Vision and Pattern Recognition*, 2021, pp. 15 859–15 869.
- [54] F. Lu, G. Chen, Y. Liu, L. Zhang, S. Qu, S. Liu, and R. Gu, "Hregnet: A hierarchical network for large-scale outdoor lidar point cloud registration," in *Proceedings of the IEEE/CVF International Conference on Computer Vision*, 2021, pp. 16 014–16 023.
- [55] H. Deng, T. Birdal, and S. Ilic, "Ppfnet: Global context aware local features for robust 3d point matching," in *Proceedings of the IEEE conference on computer vision and pattern recognition*, 2018, pp. 195–205.